VIP *Very Important Paper*

Structural Expansion of Cyclohepta[*def*]fluorene towards Azulene-Embedded Non-Benzenoid Nanographenes

Fupeng Wu+,[a, d] Ana Barragán+,[b] Aurelio Gallardo,[b] Lin Yang,[d] Kalyan Biswas,[b] David Écija,[b] Jesús I. Mendieta-Moreno,*[c] José I. Urgel,*[b] Ji Ma,*[a, d] and Xinliang Feng*[a, d]

Dedicated to Professor Maurizio Prato on the occasion of his 70th birthday

Non-benzenoid non-alternant nanographenes (NGs) have attracted increasing attention on account of their distinct electronic and structural features in comparison to their isomeric benzenoid counterparts. In this work, we present a series of unprecedented azulene-embedded NGs on Au(111) during the attempted synthesis of cyclohepta[*def*]fluorene-based high-spin non-Kekulé structure. Comprehensive scanning tunneling microscopy (STM) and non-contact atomic force microscopy (nc-AFM) evidence the structures and conforma-

tions of these unexpected products. The dynamics of the precursor bearing 9-(2,6-dimethylphenyl)anthracene and dihydro-dibenzo-cyclohepta[*def*]fluorene units and its reaction products on the surface are analyzed by density functional theory (DFT) and molecular dynamics (MD) simulations. Our study sheds light on the fundamental understanding of precursor design for the fabrication of π-extended non-benzenoid NGs on a metal surface.

Introduction

Non-benzenoid NGs have received growing attention in recent years due to their unique electronic configurations and molecular orbital characteristics, which are not shared by the benzenoid systems.[1–3] Among them, the introduction of non-alternant units (i.e., azulene or heptalene) into non-benzenoid NGs could cause local changes in strain and molecular

symmetry, thus significantly impacting their physicochemical properties.[4] Moreover, the topological transformation induced by these non-alternant moieties could also determine the electronic ground state of NGs,[5–15] affording the potential open-shell character and promising applications in organic spintronics.[16,17] As a representative example, pyrene (**a**) can be transformed into one of its non-alternant isomers, that is, cyclohepta[*def*]fluorene (**b**) (namely bis-periazulene), by replacing the inner naphthalene unit with azulene (Figure 1a), which is predicted to be an open-shell Kekulé structure with a low

[a] Dr. F. Wu,+ Dr. J. Ma, Prof. Dr. X. Feng
Max Planck Institute of Microstructure Physics
Weinberg 2, 06120 Halle (Germany)
E-mail: ji.ma@mpi-halle.mpg.de
xinliang.feng@tu-dresden.de

[b] Dr. A. Barragán,+ Dr. A. Gallardo, K. Biswas, Prof. Dr. D. Écija, Dr. J. I. Urgel
IMDEA Nanoscience
C/Faraday 9, Campus de Cantoblanco, 28049 Madrid (Spain)
E-mail: jose-ignacio.urgel@imdea.org

[c] Dr. J. I. Mendieta-Moreno
Departamento de Física Teórica de la Materia Condensada
Universidad Autónoma de Madrid
28049 Madrid (Spain)
E-mail: jesus.mendieta@uam.es

[d] Dr. F. Wu,+ L. Yang, Dr. J. Ma, Prof. Dr. X. Feng
Center for Advancing Electronics Dresden (cfaed) &
Faculty of Chemistry and Food Chemistry
Technische Universität Dresden
Mommsenstrasse 4, 01062 Dresden (Germany)

[+] These authors contributed equally to this work.

📖 Supporting information for this article is available on the WWW under https://doi.org/10.1002/chem.202301739
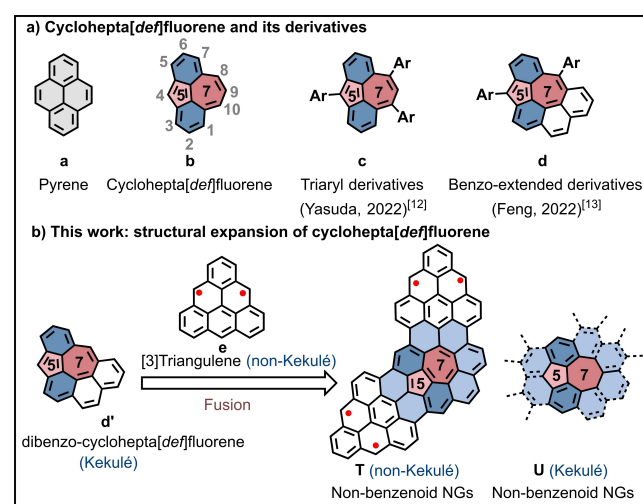
Figure 1. a) one of the seven non-alternant isomers of pyrene: cyclohepta[*def*]fluorene and its derivatives. b) targeted cyclohepta[*def*]fluorene-based non-benzenoid NGs (**T**) and conceptual structures of the unexpected products (**U**) via on-surface synthesis. Blue-filled rings denote the benzannulation of azulene, and the pink- and red-filled rings highlight the pentagonal and heptagonal rings, respectively.

Chemistry–A European Journal

Research Article
doi.org/10.1002/chem.202301739

Chemistry Europe
European Chemical
Societies Publishing

triplet ground state.[18] However, the synthesis of cyclohepta[*def*]fluorene (**b**) and its derivatives is quite challenging owing to their intrinsic instability.[19] Very recently, the solution synthesis of the triaryl derivatives of cyclohepta[*def*]fluorene (**c**) and the benzo-extended cyclohepta[*def*]fluorene derivatives (such as diaryl dibenzo-cyclohepta[*def*]fluorene, **d**) was independently reported by Yasuda's group[12] and our group.[13] It was found that the introduction of substituents onto 4,8,10-positions and dibenzo-extension onto 1,9,10-positions of cyclohepta[*def*]fluorene not only increases the molecular stability but also changes the electronic structure (Figure 1a). Experimentally, both derivatives possess the singlet ground state, contrary to the previous theoretical predictions for pristine cyclohepta[*def*]fluorene having a triplet ground state. Therefore, further exploration of the cyclohepta[*def*]fluorene derivatives is highly desirable to realize novel open-shell non-benzenoid NGs, especially the non-Kekulé structures with high-spin ground states.

The combination of solution chemistry and on-surface synthesis has emerged as a powerful approach to fabricating atomically precise graphene nanostructures, which are typically difficult to achieve using the conventional solution synthesis method.[20,21] Inspired by the recent successful on-surface synthesis of non-Kekulé [3]triangulene (**e**)[22] and Kekulé azulene-embedded NGs,[15] we devised a strategy to synthesize a novel open-shell non-Kekulé molecule (**T**) bearing a circumazulene unit on surfaces (Figure 1b) from precursor (**P**), which could be easily obtained by attaching two 9-(2,6-dimethylphenyl)anthracene (**DMPA**) units onto the dihydro-dibenzo-cyclohepta[*def*]fluorene (**d'**) core (Scheme 1). Interestingly, DFT calculations predicted that compound **T** has a triplet ground state with a singlet-triplet gap of 0.84 kcal/mol (Figure S1). However, during our investigation of utilizing precursor **P** for the synthesis of the dreaming compound **T** on Au(111), a series of unexpected azulene-embedded non-benzenoid NGs (**U**) were achieved (Figure 1). STM and nc-AFM evidence the structural properties of these unexpected products (Scheme 1, species **1**, **1'**, **2**, **3** and **3'**). It was noted that the **DMPA** segment frequently detaches from **P** (generally from the heptagon side). Furthermore, we also observed that most of the nanostructures exhibit
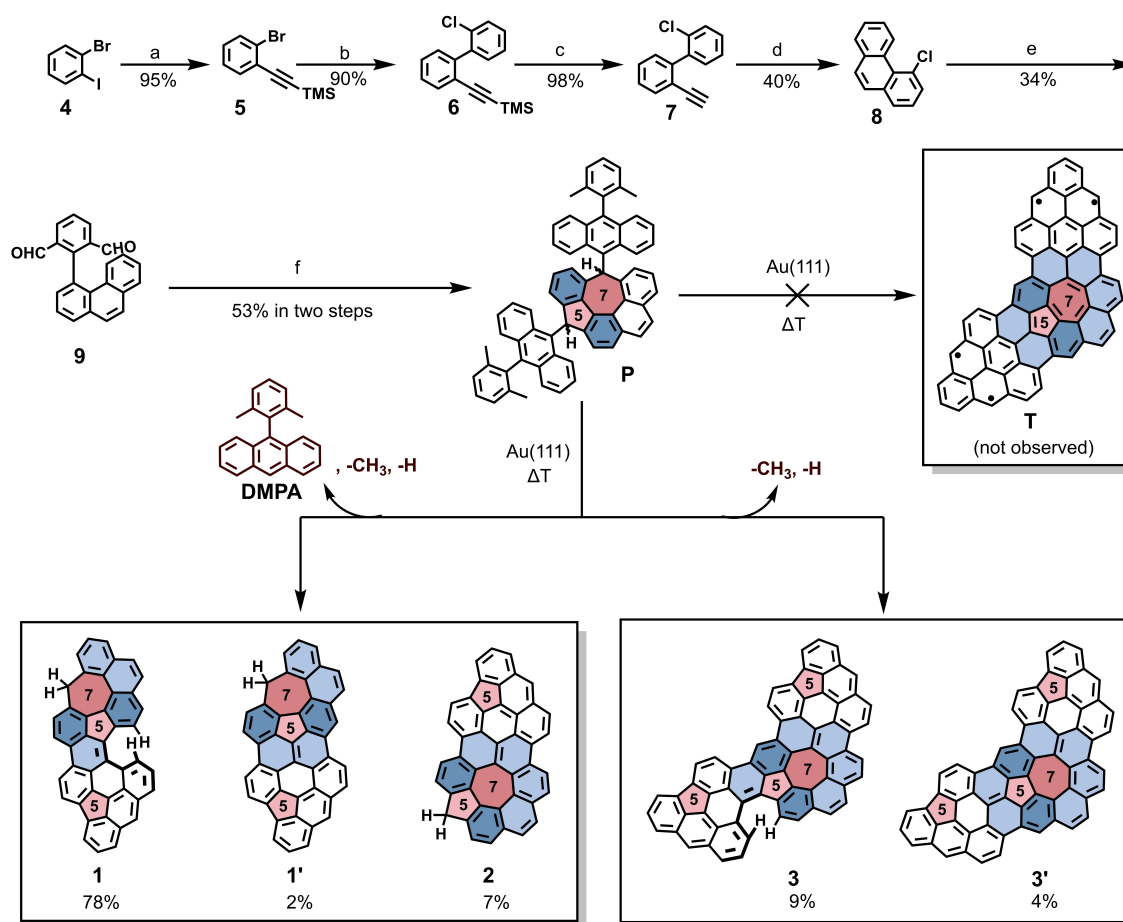
Scheme 1. Conceptual synthetic routes toward open-shell non-benzenoid NGs (**T**). In-solution synthesis of precursor **P** and on-surface reactions of precursor **P** on the Au(111) surface. Schematic representation of the reaction products **1**, **1'**, **2**, **3** and **3'** obtained after an annealing treatment of the sample. Reagents and conditions: (a) ethynyltrimethylsilane, Pd(PPh$_3$)$_2$Cl$_2$, CuI, THF/Et$_3$N, rt, 3 h. (b) (2-chlorophenyl)boronic acid, Pd(PPh$_3$)$_4$, K$_2$CO$_3$, Tol/EtOH/H$_2$O, 85 °C, 16 h. (c) K$_2$CO$_3$, MeOH/THF, 40 °C, 1 h. (d) PtCl$_2$, toluene, 110 °C, 24 h. (e) 2-(4,4,5,5-tetramethyl-1,3,2-dioxaborolan-2-yl)isophthalaldehyde, Pd(OAc)$_2$, SPhos, K$_3$PO$_4$, Tol/EtOH/H$_2$O, 80 °C, 40 h. (f) i) 9-bromo-10-(2,6-dimethylphenyl)anthracene, *n*-BuLi, THF, −78 to rt. 12 h; ii) BF$_3$·OEt$_2$, DCM, rt, 40 min. ΔT: sublimation of **P** on Au(111) surface at room temperature then subsequently annealed at 230 °C. The yield of the products on Au(111) is calculated from statistics out of 550 molecules.

Chemistry–A European Journal

Research Article
doi.org/10.1002/chem.202301739

Chemistry
Europe
European Chemical
Societies Publishing

a systematic detachment of one methyl group per **DMPA** segment, which we attribute to the two-dimensional confinement imposed by the surface. Density functional theory (DFT) and molecular dynamics (MD) simulations were performed to analyze the dynamics of the precursor and reaction products on the surface. Our study sheds light on the fundamental understanding of precursor design towards the fabrication of novel non-benzenoid NGs on surfaces.

Results and Discussion

The synthesis of **P** was carried out as shown in Scheme 1. The ((2-bromophenyl)ethynyl)trimethylsilane (**5**) was firstly obtained via Sonogashira reaction from the commercially available 1-bromo-2-iodobenzene (**4**), followed by Suzuki-coupling to afford ((2′-chloro-[1,1′-biphenyl]-2-yl)ethynyl)trimethylsilane (**6**). Then, desilylation of compound **6** gave 2-chloro-2′-ethynyl-1,1′-biphenyl (**7**) and then the PtCl$_2$-catalyzed cyclization reaction afforded 4-chlorophenanthrene (**8**). Subsequently, Suzuki-coupling of compound **8** with 2-(4,4,5,5-tetramethyl-1,3,2-dioxaborolan-2-yl)isophthalaldehyde afforded the key intermediate, 2-(phenanthren-4-yl)isophthalaldehyde (**9**).[13] After that, compound **9** was reacted with (10-(2,6-dimethylphenyl)anthracen-9-yl)lithium to give the diol, which was then subjected to Friedel–Crafts alkylation promoted by boron trifluoride ethyl etherate (BF$_3$·OEt$_2$) to afford the dihydro-precursor **P** with a yield of 53% in two steps (see the Supporting Information for detailed procedures and characterization).

After sublimation of **P** under the UHV conditions onto an atomically clean Au(111) surface held at room temperature and subsequently annealed at ~230°C, large-scale STM images (Figure 2a) reveal the presence of individual nanostructures of different sizes. First, we focused on small-sized molecules, highlighted with blue-, green- and red-colored squares in Figure 2a. High-resolution STM and nc-AFM images acquired with a CO-functionalized tip allow us to identify three distinct structural arrangements.[30] A zoomed-in nc-AFM image of the majority reaction product **1** (~80% of the studied species) is shown in Figure 2b, revealing the chemical structure of the molecule with a nonplanar conformation highlighted by the increased frequency shift (yellow and pink arrows in Figure 2b). We propose, as shown in the chemical sketch of Figure 2c, that the feature highlighted with the yellow arrow is related to the saturation with two H atoms on the apical carbon atom[21,31–34] of the heptagonal ring, while the pink arrow points to steric hindrance between two adjacent H atoms, where the expected cyclodehydrogenation reaction did not occur, lifting up a part of the **DMPA** segment. Sporadically, we observed the cyclodehydrogenation at both C–C sites, as shown in the high-resolution STM image, along with the corresponding chemical sketch of a similar molecule **1′** (Figure S2). At this point, we can conclude that the **DMPA** segment from the heptagon side tends to detach from precursor **P** in most of the studied cases. In addition, we also observed a minor amount of **2**, where the **DMPA** segment from the heptagon side is preserved after annealing and undergoes the expected cyclodehydrogenation

and ring closure reactions, while the **DMPA** from the pentagon side dissociates, as shown in Figure 2d, e. Interestingly, the nc-AFM image of **2** (Figure 2d) shows the saturation of the carbon atom located at the apex of the pentagonal ring with two H atoms, which is again marked with a yellow arrow. Importantly, this phenomenon has been recently reported for several highly reactive carbon-based nanostructures.[35]

To evaluate the tendency of the **DMPA** segments to be detached from **P** we carried out Quantum Mechanics/Molecular Mechanics (QM/MM)[36] based MD simulations analyzing two C–C distances (see Figure 2g) of the molecule adsorbed on the Au(111) surface upon annealing. To do so, we have considered the four different adsorption configurations shown in Figure 2f, that correspond to the lower energy rotamers of the single bonds of the molecule. We have also considered, based on previous studies,[37] that the hydrogen atoms located at the sp^3 carbon atoms of the five- and seven-membered rings in **P** are already cleaved by the surface at a lower temperature than the one employed in our experiment. Then, we measured the temporal evolution of distances d_a and d_b depicted in Figure 2g during an equilibrated MD simulation at 227°C, assuming that the rate of the detaching process will depend on the behavior of the reaction coordinate around its equilibrium position at a given temperature.

From the time evolution of the molecule, we calculated the probability distribution and the free energy around the equilibrium position that are shown in Figure 2h. We found in all cases a larger equilibrium position for d_a than for d_b, indicating a more double bond character for d_b and a more single-bond character for d_a, related with a smaller energy cost for its elongation and suggesting an enhanced easiness to cleavage of the molecule at the d_a bond over the d_b bond. In addition, we found that both bonds have a strain in their equilibrium distance if we compare with the same molecule in the gas phase of 0.015 Å for d_a and 0.010 Å for d_b, pointing also to a softening of the d_a. This bond cleavage will allow the central part of the molecule to planarize, increasing the molecule-surface interaction and reducing the vertical strain of the molecule.[38] The full mechanism of cleavage of C–C bonds by surface strain has been previously reported and can happen via hydrogenation[39] or mediated by a gold adatom.[40]

Next, we investigated the structural arrangement of the "croissant-like" shape species **3** and **3′**. Most of them exhibit a peripheral bright protrusion (see species **3** in STM image, Figure 3a). High-resolution STM and nc-AFM images acquired with a CO-functionalized tip allow us to determine the structure of **3**. Similarly to **1**, a sharp kink at the apex, highlighted with a pink arrow in Figure 3b can be attributed to a non-planar conformation of the molecule due to steric hindrance between two adjacent H atoms.[11,12,41] The nc-AFM inset shown in Figure 3c further confirms our assumption. This nonplanarity is clearly visible in the DFT-optimized structure (Figure 3d) of **3** on Au(111), which shows how a segment of the molecule is bent out of the plane (dihedral angle of 10.9°, with an adsorption height of 3.4 Å with respect to the underlying surface). In addition, a small amount of species **3′** was also achieved. In this case, the STM image displayed in Figure 3f lacks the bright
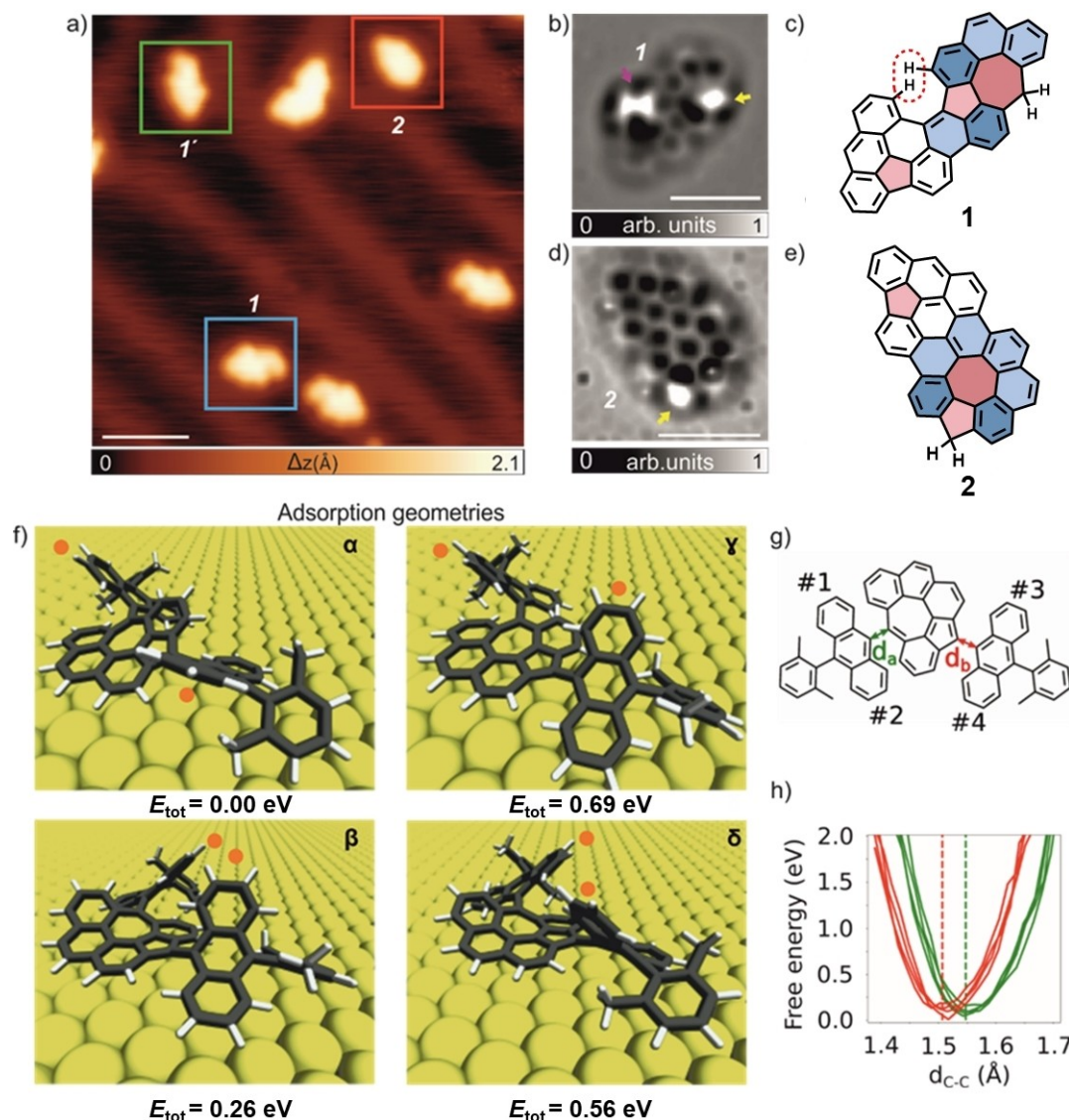
Figure 2. Identification of 1, 1' and 2 molecules after deposition on Au(111). a) Large-scale STM image ($V_b = 0.5$ V, $I_t = 50$ pA, scale bar = 2.4 nm) of the Au(111) surface showing the presence of individual nanostructures of different lengths after annealing the sample. Blue, green and red-colored squares hightlight **1**, **1'** and **2** molecules, respectively. b), d) Laplace-filtered constant-height frequency-shift nc-AFM images of product **1** (Z offset 160 pm above STM set point: $V_b = 5$ mV, $I_t = 50$ pA, scale bar = 1 nm), and of product **2** (Z offset 180 pm above STM set point: $V_b = 5$ mV, $I_t = 50$ pA, scale bar = 1 nm), respectively, acquired with a CO-functionalized tip. Pink and yellow arrows indicate the saturation with two H atoms on the apical carbon atom of the heptagonal ring and the steric hindrance between two adjacent H atoms, respectively. c) and e) Chemical sketch of products **1** and **2**, respectively. f) QM/MM relaxed geometry of the four adsorption configurations considered. According to the nomenclature shown in panel (g), where four benzene rings are labelled as #1, #2, #3 and #4: α presents two protrude rings #1 and #3, β #2 and #4, γ #1 and #4 and δ #2 and #3. In all the images, the protruding benzene rings are indicated with an orange dot for clarity. The indicated E_{tot} stands for total energy. g) Scheme of the precursor after the adsorption and definition of labels and reaction coordinates for the Free energy shown in panel (h). h) Free energy vs d_a and d_b C–C distances. The dashed lines indicate the average position of the Free energy minima for d_a (at 1.55 Å) and d_b (at 1.51 Å).

protrusion observed for **3**. Figure 3g shows the high-resolution STM image of **3'** where only smooth molecular apexes are observed, which together with the DFT-optimized structure (Figure 3h) of the molecule confirms its chemical structure on the Au(111) surface. To explore the electronic structure of both species, we performed scanning tunneling spectroscopy (STS) measurements. Voltage-dependent differential conductance spectra (dI/dV vs. V) show features in the density of states at −0.87 V and +1.11 V for **3** and −0.91 V and +1.20 V for **3'**, which are attributed to the highest occupied and the lowest

unoccupied molecular orbitals (HOMO and LUMO) of the molecules (see Figure S3). Therefore, the measured electronic gaps of these molecules are considerably large (~2 eV) on Au(111).

To have a better understanding of the origin of species **3** and **3'**, whose on-surface synthesis has skipped the **DMPA** removal, and to comprehend the selectivity in the ring closure, we analyzed the distances of the possible bonds created after the cyclodehydrogenation (d_{1-4}, depicted in Figure 4a for the four considered adsorption configurations) with the same
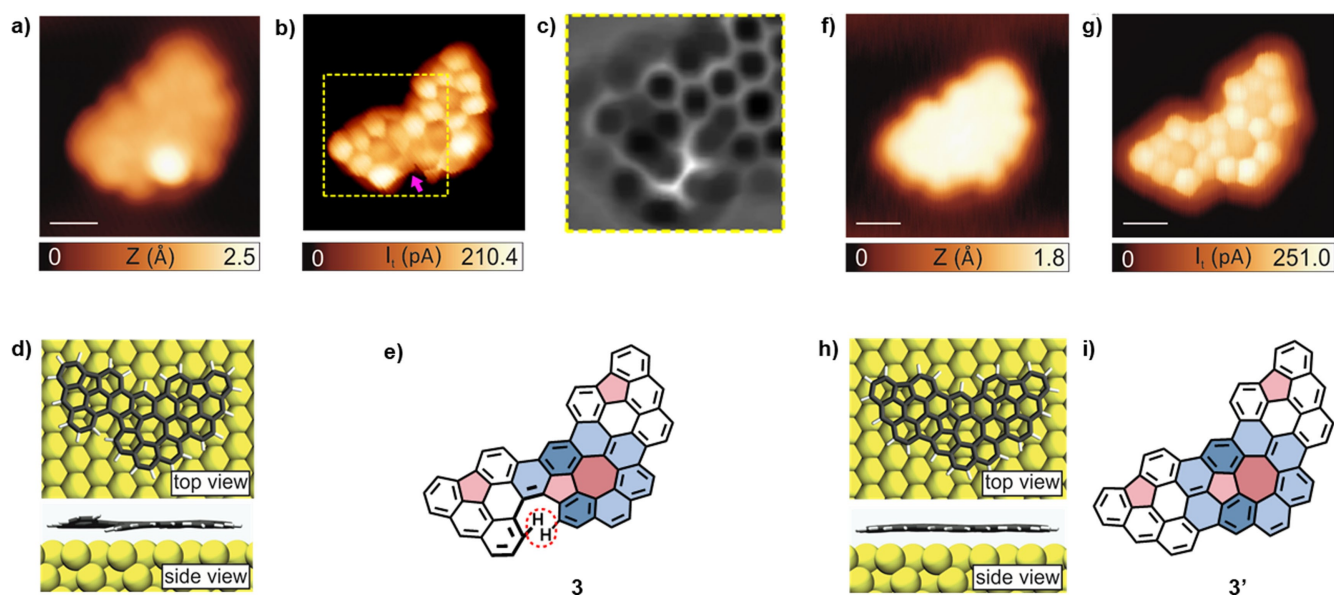
Figure 3. On-surface synthesis of species **3** and **3'** on Au(111). a), b) and f), g) High-resolution constant-current and constant-height STM images acquired with a CO-functionalized tip of products **3** and **3'**, respectively. The panel c) shows the Laplace-filtered constant-height frequency-shift nc-AFM image of the dashed yellow rectangle, showing the steric hindrance of the two adjacent H atoms. d), e) and h), i) DFT-optimized structures and chemical sketches of products **3** and **3'**, respectively. Scanning parameters: a) $V_b = -1.5$ V, $I_t = 35$ pA, scale bar $= 6.0$ Å; b) $V_b = 5$ mV, $I_t = 50$ pA, scale bar $= 4.0$ Å; e) $V_b = 5$ mV, $I_t = 50$ pA, scale bar $= 6.0$ Å and f) $V_b = 5$ mV, $I_t = 50$ pA, scale bar $= 4.2$ Å.
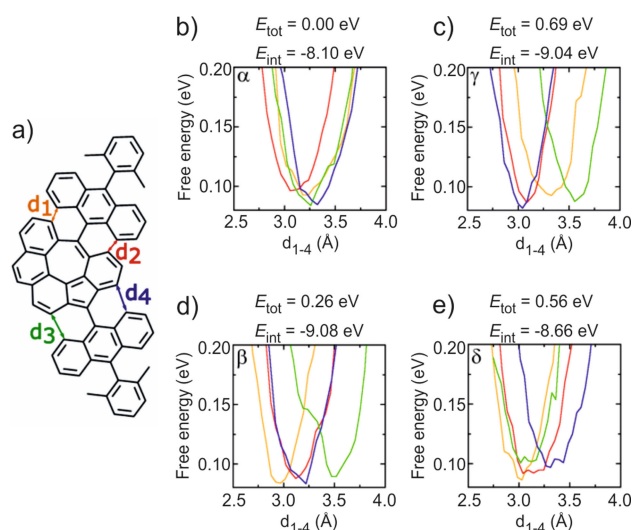
Figure 4. a) Definition of the reaction coordinates d_1, d_2, d_3 and d_4. b)–e) Free energy vs d_1, d_2, d_3 and d_4 calculated for the b) α, c) γ, d) β and e) δ structures. The indicated E_{tot} and E_{int} stand for total energy and molecule-surface interaction energy respectively.

approach used for d_a and d_b. Panels b-e of Figure 4 show the Free energy around the equilibrium position of d_{1-4} for the four considered configurations. Focusing on configurations α and β in Figure 4, which correspond to the two more stable configurations, we can relate the shift of the equilibrium distances with the selectivity of the cyclodehydrogenation that leads to species **3** and **3'**. In contrast to d_a and d_b distances related to the **DMPA** cleavage, for the ring closures we observed a different behavior for each configuration. In the case of configuration α, all four distances show a similar equilibrium value, indicating that they are all equally likely to undergo

cyclodehydrogenation. This case could be the one leading to species **3'**. On the other hand, for the results shown in the configuration β, the geometry of the adsorbed molecule shifts the equilibrium value of d_3 towards higher values, hindering the corresponding dehydrogenation.

With these results, we can observe the effect of the surface strain in a non-planar molecule changes certain vibrational modes along the four reaction coordinates. Surface strain will change in each absorption conformation and different vibrational modes will be suppressed, shifted or enhanced, affecting the transformation process. For instance, we observed that the absorption geometries β and γ find their capability to create a bond along d_3 strongly suppressed with respect to d_1, d_2 and d_4. We can relate this behavior with the vertical position of the anthracene moiety on the surface, since in these cases the ring containing the C of d_3 distance lie planar and close to the surface, limiting their out-of-plane vibrations. On the other hand, in configuration α, the ring of the anthracene moiety or the corresponding ring on the central part of the molecules that may form any of the four possible bonds is free to move out of plane, enhancing the vibrational modes along the reaction coordinates. In a similar fashion, in configuration δ, the rings that correspond to distance d_4 find their out-of-plane vibrations limited, inhibiting the formation of the corresponding bond. Here we propose a vertical strain-driven mechanism of cyclodehydrogenation also reported in a previous paper.[42] In addition, for cyclodehydrogenation reactions, it has also been proposed that surface adatoms can play an important role in decreasing the reaction barrier and promoting the bond formation.[43,44]

Finally, a comment regarding the systematic detachment of one methyl group per **DMPA** segment for all the observed

Chemistry–A European Journal

Research Article
doi.org/10.1002/chem.202301739

Chemistry Europe
European Chemical
Societies Publishing

species is appropriate. We hypothesized that the C–H activation of the methyl groups pointing upwards (see adsorption geometries in Figure 2) expected to undergo the oxidative ring closure, does not take place due to their large distance with respect to the catalyzing gold surface (see Figure S4 and S5 for the adsorption geometry of **P** after the cyclodehydrogenation corresponding to the reaction coordinates d_1, d_2, and d_4 and species **3** with the pentagon rings formed at different positions).[5,8,45,46]

Conclusions

In conclusion, we have demonstrated the on-surface synthesis towards distinct cyclohepta[*def*]fluorene-based structures originated from precursor **P**. A series of unexpected azulene-embedded non-benzenoid NGs (**1**, **1′**, **2**, **3** and **3′**) were achieved on the Au(111) surface. Their structures have been clearly elucidated by STM and nc-AFM. All these unexpected products are azulene-embedded NGs containing pentagonal and heptagonal rings. In addition, product **3′** also contains a circumazulene unit. MD results show a clear preference for the **DMPA** segment to detach from the heptagon side, enhanced by the molecule-surface interaction. The calculations also indicate a vertical strain-driven selectivity in the cyclodehydrogenation process, suggesting this as a key factor of the reaction process. Our results can pave the way for the fundamental understanding of precursor design towards the fabrication of non-benzenoid NGs containing multiple fused pentagon-heptagon pairs, as well as azulene-embedded graphene nanoribbons.

Supporting Information

Additional references cited within the Supporting Information.[47–59]

Conflict of Interests

The authors declare no conflict of interest.

Data Availability Statement

The data that support the findings of this study are available from the corresponding author upon reasonable request.

[1] H. Miyoshi, S. Nobusue, A. Shimizu, Y. Tobe, *Chem. Soc. Rev.* **2015**, *44*, 6560–6577.
[2] A. Konishi, M. Yasuda, *Chem. Lett.* **2021**, *50*, 195–212.
[3] Y. Tobe, *Chem. Rec.* **2015**, *15*, 86–96.
[4] S. H. Pun, Q. Miao, *Acc. Chem. Res.* **2018**, *51*, 1630–1642.
[5] K. Biswas, L. Yang, J. Ma, A. Sánchez-Grande, Q. Chen, K. Lauwaet, J. M. Gallego, R. Miranda, D. Écija, P. Jelínek, X. Feng, J. I. Urgel, *J. Nanomater.* **2022**, *12*, 224.
[6] C. Li, Y. Liu, Y. Liu, F.-H. Xue, D. Guan, Y. Li, H. Zheng, C. Liu, J. Jia, P.-N. Liu, D.-Y. Li, S. Wang, *CCS Chem.* **2023**, *5*, 695–703.
[7] H. Xin, B. Hou, X. Gao, *Acc. Chem. Res.* **2021**, *54(7)*, 1737–1753.
[8] S. Mishra, D. Beyer, R. Berger, J. Liu, O. Gröning, J. I. Urgel, K. Müllen, P. Ruffieux, X. Feng, R. Fasel, *J. Am. Chem. Soc.* **2020**, *142*, 1147–1152.
[9] A. Konishi, K. Horii, D. Shiomi, K. Sato, T. Takui, M. Yasuda, *J. Am. Chem. Soc.* **2019**, *141*, 10165–10170.
[10] J. Liu, S. Mishra, C. A. Pignedoli, D. Passerone, J. I. Urgel, A. Fabrizio, T. G. Lohr, J. Ma, H. Komber, M. Baumgarten, C. Corminboeuf, R. Berger, P. Ruffieux, K. Müllen, R. Fasel, X. Feng, *J. Am. Chem. Soc.* **2019**, *141*, 12011–12020.
[11] R. Liu, Y. Fu, F. Wu, F. Liu, J.-J. Zhang, L. Yang, A. A. Popov, J. Ma, X. Feng, *Angew. Chem. Int. Ed.* **2023**, *62*, e202219091; *Angew. Chem.* **2023**, *135*, e202219091.
[12] K. Horii, R. Kishi, M. Nakano, D. Shiomi, K. Sato, T. Takui, A. Konishi, M. Yasuda, *J. Am. Chem. Soc.* **2022**, *144*, 3370–3375.
[13] F. Wu, J. Ma, F. Lombardi, Y. Fu, F. Liu, Z. Huang, R. Liu, H. Komber, D. I. Alexandropoulos, E. Dmitrieva, T. G. Lohr, N. Israel, A. A. Popov, J. Liu, L. Bogani, X. Feng, *Angew. Chem. Int. Ed.* **2022**, *61*, e202202170; *Angew. Chem.* **2022**, *134*, e202202170.
[14] J. Ma, X. Feng, *Diradicaloids, Chapter 9*, Jenny Stanford Publishing, **2022**, 353–417.
[15] a) S. Mishra, T. G. Lohr, C. A. Pignedoli, J. Liu, R. Berger, J. I. Urgel, K. Müllen, X. Feng, P. Ruffieux, R. Fasel, *ACS Nano* **2018**, *12*, 11917–11927; b) J. Hieulle, E. Carbonell-Sanromà, M. Vilas-Varela, A. Garcia-Lekue, E. Guitián, D. Peña, J. I. Pascual, *Nano Lett.* **2018**, *18(1)*, 418–423.
[16] F. Lombardi, J. Ma, D. I. Alexandropoulos, H. Komber, J. Liu, W. K. Myers, X. Feng, L. Bogani, *Chem* **2021**, *7*, 1363–1378.
[17] F. Lombardi, A. Lodi, J. Ma, J. Liu, M. Slota, A. Narita, W. K. Myers, K. Müllen, X. Feng, L. Bogani, *Science* **2019**, *366*, 1107–1110.
[18] M. Nendel, B. Goldfuss, K. N. Houk, K. Hafner, U. Grieser, *Theor. Chem. Acc.* **1999**, *102*, 397–400.
[19] A. Konishi, K. Horii, M. Yasuda, *J. Phys. Org. Chem.* **2023**, *36*, e4495.
[20] Q. Shen, H.-Y. Gao, H. Fuchs, *Nano Today* **2017**, *13*, 77–96.
[21] P. Ruffieux, S. Wang, B. Yang, C. Sánchez-Sánchez, J. Liu, T. Dienel, L. Talirz, P. Shinde, C. A. Pignedoli, D. Passerone, T. Dumslaff, X. Feng, K. Müllen, R. Fasel, *Nature* **2016**, *531*, 489–492.
[22] N. Pavliček, A. Mistry, Z. Majzik, N. Moll, G. Meyer, D. J. Fox, L. Gross, *Nat. Nanotechnol.* **2017**, *12*, 308–311.

Chemistry–A European Journal

Research Article
doi.org/10.1002/chem.202301739

Chemistry Europe
European Chemical
Societies Publishing

[23] S. Mishra, D. Beyer, K. Eimre, J. Liu, R. Berger, O. Gröning, C. A. Pignedoli, K. Müllen, R. Fasel, X. Feng, P. Ruffieux, *J. Am. Chem. Soc.* **2019**, *141*, 10621–10625.

[24] J. Su, M. Telychko, P. Hu, G. Macam, P. Mutombo, H. Zhang, Y. Bao, F. Cheng, Z.-Q. Huang, Z. Qiu, S. J. R. Tan, H. Lin, P. Jelínek, F.-C. Chuang, J. Wu, J. Lu, *Sci. Adv.* **2019**, *5*, eaav7717.

[25] J. Su, M. Telychko, S. Song, J. Lu, *Angew. Chem. Int. Ed.* **2020**, *59*, 7658–7668; *Angew. Chem.* **2020**, *132*, 7730–7740.

[26] J. Su, W. Fan, P. Mutombo, X. Peng, S. Song, M. Ondráček, P. Golub, J. Brabec, L. Veis, M. Telychko, P. Jelínek, J. Wu, J. Lu, *Nano Lett.* **2021**, *21*, 861–867.

[27] S. Mishra, K. Xu, K. Eimre, H. Komber, J. Ma, C. A. Pignedoli, R. Fasel, X. Feng, P. Ruffieux, *Nanoscale* **2021**, *13*, 1624–1628.

[28] J. Hieulle, S. Castro, N. Friedrich, A. Vegliante, F. R. Lara, S. Sanz, D. Rey, M. Corso, T. Frederiksen, J. I. Pascual, D. Peña, *Angew. Chem. Int. Ed.* **2021**, *60*, 25224–25229; *Angew. Chem.* **2021**, *133*, 25428–25433.

[29] S. Mishra, G. Catarina, F. Wu, R. Ortiz, D. Jacob, K. Eimre, J. Ma, C. A. Pignedoli, X. Feng, P. Ruffieux, J. Fernández-Rossier, R. Fasel, *Nature* **2021**, *598*, 287–292.

[30] L. Gross, *Nat. Chem.* **2011**, *3*, 273–278.

[31] M. Di Giovannantonio, K. Eimre, A. V. Yakutovich, Q. Chen, S. Mishra, J. I. Urgel, C. A. Pignedoli, P. Ruffieux, K. Müllen, A. Narita, R. Fasel, *J. Am. Chem. Soc.* **2019**, *141*, 12346–12354.

[32] K. Biswas, M. Urbani, A. Sánchez-Grande, D. Soler-Polo, K. Lauwaet, A. Matěj, P. Mutombo, L. Veis, J. Brabec, K. Pernal, J. M. Gallego, R. Miranda, D. Écija, P. Jelínek, T. Torres, J. I. Urgel, *J. Am. Chem. Soc.* **2022**, *144*, 12725–12731.

[33] X. Xu, M. Di Giovannantonio, J. I. Urgel, C. A. Pignedoli, P. Ruffieux, K. Müllen, R. Fasel, A. Narita, *Nano Res.* **2021**, *14*, 4754–4759.

[34] X. Su, C. Li, Q. Du, K. Tao, S. Wang, P. Yu, *Nano Lett.* **2020**, *20*, 6859–6864.

[35] a) S. Cheng, Z. Xue, C. Li, Y. Liu, L. Xiang, Y. Ke, K. Yan, S. Wang, P. Yu, *Nat. Commun.* **2022**, *13*, 1705; b) J. Liu, X. Feng, *Angew. Chem. Int. Ed.* **2020**, *59*, 23386–23401; *Angew. Chem.* **2020**, *132*, 23591–23607.

[36] J. I. Mendieta-Moreno, R. C. Walker, J. P. Lewis, P. Gómez-Puertas, J. Mendieta, J. Ortega, *J. Chem. Theory Comput.* **2014**, *10*, 2185–2193.

[37] A. Kinikar, M. Di Giovannantonio, J. I. Urgel, K. Eimre, Z. Qiu, Y. Gu, E. Jin, A. Narita, X.-Y. Wang, K. Müllen, P. Ruffieux, C. A. Pignedoli, R. R. Fasel, *Nat. Synth.* **2022**, *1*, 289–296.

[38] a) J. Su, X. Wu, S. Song, M. Telychko, J. Lu, *Nanoscale* **2020**, *12*, 7500–7508; b) L. Li, S. Mahapatra, D. Liu, Z. Lu, N. Jiang, *ACS Nano* **2021**, *15*, 3578–3585.

[39] C. Wäckerlin, A. Gallardo, A. Mairena, M. Baljozović, A. Cahlík, A. Antalík, J. Brabec, L. Veis, D. Nachtigallová, P. Jelínek, K.-H. Ernst, *ACS Nano* **2020**, *14*, 16735–16742.

[40] J. I. Mendieta-Moreno, B. Mallada, B. De la Torre, T. Cadart, M. Kotora, P. Jelínek, *Angew. Chem. Int. Ed.* **2022**, *61*, e202208010; *Angew. Chem.* **2022**, *134*, e202208010.

[41] T. G. Lohr, J. I. Urgel, K. Eimre, J. Liu, M. Di Giovannantonio, S. Mishra, R. Berger, P. Ruffieux, C. A. Pignedoli, R. Fasel, X. Feng, *J. Am. Chem. Soc.* **2020**, *142*, 13565–13572.

[42] B. Mallada, B. de la Torre, J. I. Mendieta-Moreno, D. Nachtigallová, A. Matěj, M. Matoušek, P. Mutombo, J. Brabec, L. Veis, T. Cadart, M. Kotora, P. Jelínek, *J. Am. Chem. Soc.* **2021**, *143*, 14694–14702.

[43] B. de la Torre, A. Matěj, A. Sánchez-Grande, B. Cirera, B. Mallada, E. Rodríguez-Sánchez, J. Santos, J. I. Mendieta-Moreno, S. Edalatmanesh, K. Lauwaet, M. Otyepka, M. Medveď, Á. Buendía, R. Miranda, N. Martín, P. Jelínek, D. Écija, *Nat. Commun.* **2020**, *11*, 4567.

[44] J. Björk, C. Sánchez-Sánchez, Q. Chen, C. A. Pignedoli, J. Rosen, P. Ruffieux, X. Feng, A. Narita, K. Müllen, R. Fasel, *Angew. Chem. Int. Ed.* **2022**, *61*, e202212354; *Angew. Chem.* **2022**, *134*, e202212354.

[45] K. Biswas, J. I. Urgel, M. R. Ajayakumar, J. Ma, A. Sánchez-Grande, S. Edalatmanesh, K. Lauwaet, P. Mutombo, J. M. Gallego, R. Miranda, P. Jelínek, X. Feng, D. Écija, *Angew. Chem. Int. Ed.* **2022**, *61*, e202114983; *Angew. Chem.* **2022**, *134*, e202114983.

[46] Y. Zhao, K. Jiang, C. Li, Y. Liu, C. Xu, W. Zheng, D. Guan, Y. Li, H. Zheng, C. Liu, W. Luo, J. Jia, X. Zhuang, S. Wang, *J. Am. Chem. Soc.* **2020**, *142*, 18532–18540.

[47] Y.-K. Zhang, J. J. Plattner, E. E. Easom, D. Waterson, M. Ge, Z. Li, L. Li, Y. Jian, *Tetrahedron Lett.* **2011**, *52*, 3909–3911.

[48] L. Valenta, M. Mayländer, P. Kappeler, O. Blacque, T. Šolomek, S. Richert, M. Juríček, *Chem. Commun.* **2022**, *58*, 3019–3022.

[49] F. J. Giessibl, *Appl. Phys. Lett.* **2000**, *76*, 1470–1472.

[50] L. Bartels, G. Meyer, K. H. Rieder, D. Velic, E. Knoesel, A. Hotzel, M. Wolf, G. Ertl, *Phys. Rev. Lett.* **1998**, *80*, 2004–2007.

[51] I. Horcas, R. Fernández, J. M. Gómez-Rodríguez, J. Colchero, J. Gómez-Herrero, A. M. Baro, *Rev. Sci. Instrum.* **2007**, *78*.

[52] J. I. Mendieta-Moreno, R. C. Walker, J. P. Lewis, P. Gómez-Puertas, J. Mendieta, J. Ortega, *J. Chem. Theory Comput.* **2014**, *10*, 2185–2193.

[53] D. A. Case, H. M. Aktulga, K. Belfon, I. Y. Ben-Shalom, J. T. Berryman, S. R. Brozell, D. S. Cerutti, T. E. Cheatham, III, G. A. Cisneros, V. W. D. Cruzeiro, T. A. Darden, N. Forouzesh, G. Giambaşu, T. Giese, M. K. Gilson, H. Gohlke, A. W. Goetz, J. Harris, S. Izadi, S. A. Izmailov, K. Kasavajhala, M. C. Kaymak, E. King, A. Kovalenko, T. Kurtzman, T. S. Lee, P. Li, C. Lin, J. Liu, T. Luchko, R. Luo, M. Machado, V. Man, M. Manathunga, K. M. Merz, Y. Miao, O. Mikhailovskii, G. Monard, H. Nguyen, K. A. O'Hearn, A. Onufriev, F. Pan, S. Pantano, R. Qi, A. Rahnamoun, D. R. Roe, A. Roitberg, C. Sagui, S. Schott-Verdugo, A. Shajan, J. Shen, C. L. Simmerling, N. R. Skrynnikov, J. Smith, J. Swails, R. C. Walker, J. Wang, J. Wang, H. Wei, X. Wu, Y. Wu, Y. Xiong, Y. Xue, D. M. York, S. Zhao, Q. Zhu, P. A. Kollman (2023), Amber **2023**, University of California, San Francisco.

[54] H. Heinz, T.-J. Lin, R. Kishore Mishra, F. S. Emami, *Langmuir* **2013**, *29*, 1754–1765.

[55] J. Lewis, P. Jelenik, J. Ortega, A. Demkov, D. Trabada, B. Haycock, A. G. Wang Ha, J. Tomfohr, E. Abad, *Phys. Status Solidi B* **1989**, *248*.

[56] A. D. Becke, *Phys. Rev. A* **1988**, *38*, 3098.

[57] C. Lee, W. Yang, R. G. Parr, *Phys. Rev. B* **1988**, *37*, 785.

[58] C. Lee, W. Yang, R. G. Parr, *Phys. Rev. B* **1988**, *37*, 785–789.

[59] M. A. Basanta, Y. J. Dappe, P. Jelínek, J. Ortega, *Comput. Mater. Sci.* **2007**, *39*, 759–766.

RESEARCH ARTICLE

A series of unprecedented non-benzenoid NGs containing cyclohepta[*def*]fluorine unit are obtained via on-surface synthesis on Au(111). Scanning tunneling microscopy and non-contact atomic force microscopy evidence their structures and conformations. Moreover, the dynamics of the precursor and its reaction products on the surface are analyzed by DFT and MD simulations.

Cyclohepta[*def*]fluorene Derivatives
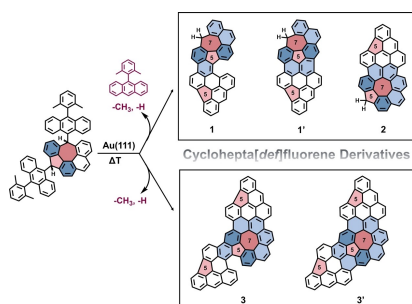
Dr. F. Wu, Dr. A. Barragán, Dr. A. Gallardo, L. Yang, K. Biswas, Prof. Dr. D. Écija, Dr. J. I. Mendieta-Moreno*, Dr. J. I. Urgel*, Dr. J. Ma*, Prof. Dr. X. Feng*

1 – 8

Structural Expansion of Cyclohepta[*def*]fluorene towards Azulene-Embedded Non-Benzenoid Nanographenes